UNIVERSITYOF BIRMINGHAM

University of Birmingham
Research at Birmingham

Hyperpolarized 13C MRI

Grist, James T; Miller, Jack J; Zaccagna, Fulvio; McLean, Mary A; Riemer, Frank; Matys, Tomasz; Tyler, Damian J; Laustsen, Christoffer; Coles, Alasdair J; Gallagher, Ferdia A

[Link to publication on Research at Birmingham portal](#)

Review Article

JCBFM

Hyperpolarized ^{13}C MRI: A novel approach for probing cerebral metabolism in health and neurological disease

James T Grist[1,2,]*[ ] , Jack J Miller[3,4,5,]*, Fulvio Zaccagna[2,]*,
Mary A McLean[2,6], Frank Riemer[2], Tomasz Matys[2],
Damian J Tyler[3,5], Christoffer Laustsen[7], Alasdair J Coles[8] and
Ferdia A Gallagher[2]

Abstract

Cerebral metabolism is tightly regulated and fundamental for healthy neurological function. There is increasing evidence that alterations in this metabolism may be a precursor and early biomarker of later stage disease processes. Proton magnetic resonance spectroscopy (^{1}H-MRS) is a powerful tool to non-invasively assess tissue metabolites and has many applications for studying the normal and diseased brain. However, the technique has limitations including low spatial and temporal resolution, difficulties in discriminating overlapping peaks, and challenges in assessing metabolic flux rather than steady-state concentrations. Hyperpolarized carbon-13 magnetic resonance imaging is an emerging clinical technique that may overcome some of these spatial and temporal limitations, providing novel insights into neurometabolism in both health and in pathological processes such as glioma, stroke and multiple sclerosis. This review will explore the growing body of pre-clinical data that demonstrates a potential role for the technique in assessing metabolism in the central nervous system. There are now a number of clinical studies being undertaken in this area and this review will present the emerging clinical data as well as the potential future applications of hyperpolarized ^{13}C magnetic resonance imaging in the brain, in both clinical and pre-clinical studies.

Introduction: metabolic studies of the brain using proton and carbon-13 MR spectroscopy

Proton Magnetic Resonance Spectroscopy (^{1}H-MRS) is a non-invasive technique to probe *in vivo* metabolism that has been applied in a number of neurological diseases such as brain tumors, multiple sclerosis (MS), traumatic brain injury (TBI), stroke, and dementia.[1–5] However, the millimolar concentration of most metabolites in human tissues results in a relatively low signal-to-noise ratio (SNR), therefore limiting the spatial and temporal resolution that can be achieved within a clinically acceptable scan time.[6] Metabolites that are commonly probed with ^{1}H-MRS include choline, creatine, N-acetyl aspartate, and lactate (markers of cellular

[1]Institute of Cancer and Genomic Sciences, University of Birmingham, Birmingham, UK
[2]Department of Radiology, University of Cambridge, Cambridge, UK
[3]Department of Physiology, Anatomy, and Genetics, University of Oxford, Oxford, UK
[4]Department of Physics, Clarendon Laboratory, University of Oxford, Oxford, UK
[5]Oxford Centre for Clinical Magnetic Resonance Research, John Radcliffe Hospital, Oxford, UK
[6]CRUK Cambridge Institute, Cambridge, UK
[7]MR Research Centre, Aarhus University, Aarhus, Denmark
[8]Department of Clinical Neurosciences, University of Cambridge, Cambridge, UK

*These authors contributed equally to this work.

Corresponding author:
Ferdia A Gallagher, Department of Radiology, University of Cambridge, Cambridge, UK.
Email: fag1000@cam.ac.uk

proliferation, mitochondrial metabolism, neuronal integrity, and glycolytic metabolism, respectively). However, other metabolites such as glutamate, glutamine, myo-inositol, and hypotaurine (which are involved in neurotransmission, amino acid metabolism and act as osmolytes; concentrations of these molecules vary depending on cellular composition and can be used to help distinguish tumor subtypes[7]) are more challenging to quantify due to overlapping peaks on the ^{1}H-MRS spectrum at conventional clinical (1.5–3 T) field strengths.[6] Although the spatial distribution of these metabolites can be imaged with MR spectroscopic imaging techniques, this is usually at low spatial resolution (approximately 3–8 mL single voxel volume[8]) and is time consuming. The metabolite concentrations derived from ^{1}H-MRS usually reflect steady-state tissue concentrations, which although important, do not reflect enzymatic flux or exchange which is complementary additional information.

Carbon-13-MRS (^{13}C-MRS) has also been utilized to non-invasively probe cerebral metabolic pathways such as the tricarboxylic acid (TCA) cycle, in both health and disease in a more detailed manner through the injection of ^{13}C-labelled endogenous tracers such as glucose, whereby incorporation and metabolism of the ^{13}C label can be followed dynamically, allowing metabolic pathways to be deconvolved in ways which complement the detection of steady-state metabolic pool sizes.[9–13] However, despite the ^{13}C enrichment of the injected molecule and the negligible ^{13}C signal from unlabelled background metabolites, the SNR is still very low, which is partly due to the less favorable magnetic properties of ^{13}C compared to [1]H (i.e. a lower gyromagnetic ratio and typically long nuclear T_1). This also restricts the achievable spatial and temporal resolutions of the technique and limits the technique to the research setting. Metabolic imaging of endogenous ^{13}C metabolites is currently challenging at clinical field strengths; however, the increasing number of high field MR systems at 7 T or above offers the potential of using ^{13}C-MRS for thermal experiments in humans.[14,15]

Dynamic nuclear polarization or hyperpolarized carbon-13 MRI

Dynamic nuclear polarization (DNP) has been used to overcome the limitations of ^{13}C-MRS by providing a temporary increase in SNR of between 10,000 and 100,000-fold, allowing the uptake and metabolic conversion of physiologically relevant substrates to be imaged.[16–20] This advance has opened up the potential of the technique to image tissue metabolism in real-time at high resolution (2–4 s temporal resolution and with ~8 mL voxel volume[21]) and also offers the

possibility of using it as a clinical tool to stratify patients based on their metabolic phenotype and detect changes in metabolism in response to treatment. Early clinical studies have focused on the use of hyperpolarized pyruvate to probe both glycolysis and TCA metabolism for oncological, renal, and cardiac metabolism.[22–31] This review explores the application of ^{13}C-MRI to cerebral imaging and its future potential in the clinic.

Requirements for clinical hyperpolarized studies

Clinical hyperpolarized ^{13}C-MRI requires a dedicated sterile facility to fill pharmacy kits (a small sterile vial containing pyruvate, a syringe with water to dissolve the pyruvate and buffer to neutralize the solution as shown in Figure 1 [32]). The filled kit then undergoes hyperpolarization using a commercial clinical system (SPINlab, GE Healthcare, see Figure 2) and is quality checked for parameters such as pH, temperature and polarization level, before intravenous injection over 5–6 s (~5 ml/s) of ~250 mmol/L hyperpolarized ^{13}C-pyruvate at 0.4 ml/kg body weight. ~250 mmol/L has been widely used for the initial clinical studies based on the concentration of neat pyruvic acid and the volume of heated water required to dissolve this rapidly and this concentration has shown a good toxicity profile. This produces an approximate intravascular concentration of ~1–2 mmol/L after injection but a tissue concentration which is an order of magnitude smaller (~0.1 mmol/L) and similar to the physiological concentration of
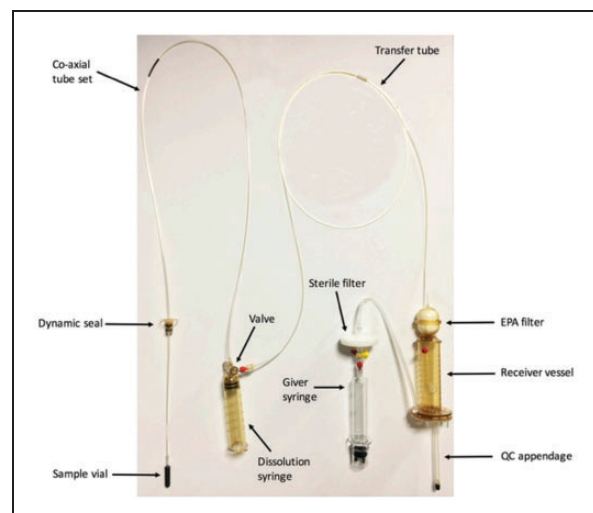

Figure 1. A sterile fluid path for clinical studies. The fluid path contains pyruvate (in sample vial), water for injection (dissolution syringe), and a neutralization medium (held in the receiver vessel). The filter on the receiver vessel removes the electron paramagnetic agent (EPA) prior to quality control (QC). Figure adapted from Park et al.[21]
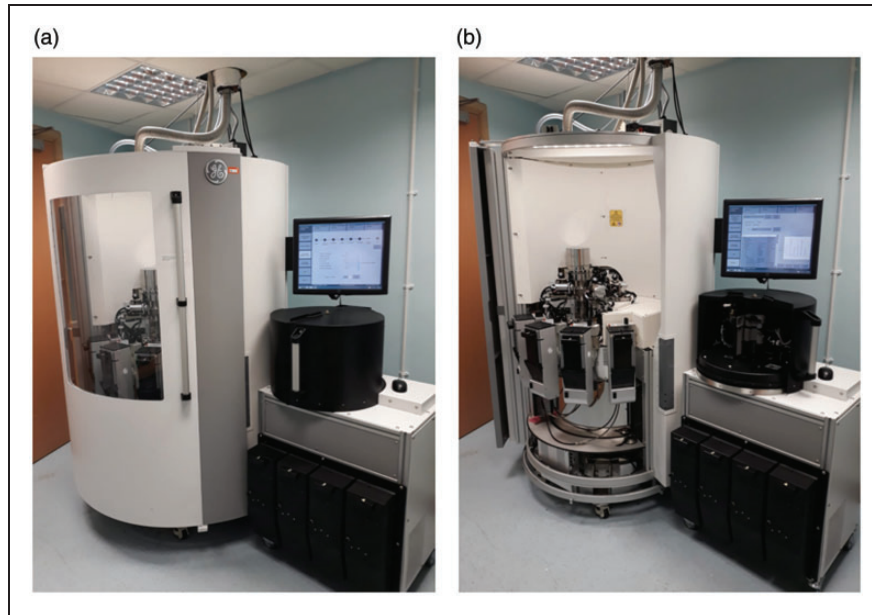
Figure 2. The clinical "SPINlab" hyperpolariser system exterior (a) and interior (b). The Quality Control (QC) unit is shown on the right of each image, and the hyperpolarizer on the left. The system is sited next to a clinical scanner with a hatch in the wall for the delivery of the hyperpolarized sample; this will be placed into a syringe driver and injected into the patient.

endogenous pyruvate.[33] Lower doses may be possible in future but produce lower signal, because signal varies linearly with the amount of the injected tracer. Imaging the ^{13}C-labelled metabolites is undertaken using dedicated MRI coils and sequences which acquire rapid images of the injected substrate and the metabolites that form from it in real time.[21,34–40] Imaging must be performed rapidly, as the increased polarization is transient and decays with the T_1 of the labelled ^{13}C (less than one minute in blood), and is therefore a limitation for *in vivo* measurements of slow enzymatic reactions.

Cellular localization and quantification of cerebral pyruvate metabolism

Metabolism can be quantified by modelling the dynamics of signal acquired from the substrate (e.g. pyruvate) and its products (e.g. lactate or bicarbonate) to infer enzymatic activity.[41] Pyruvate resides at the junction of several important biochemical pathways such as the exchange to lactate in the cytosol, catalyzed by the enzyme lactate dehydrogenase (LDH), or the irreversible conversion to carbon dioxide, catalyzed by the mitochondrial enzyme pyruvate dehydrogenase (PDH). The labelled carbon dioxide subsequently exchanges with the bicarbonate pool, catalyzed very rapidly by the enzyme carbonic anhydrase (CA); this bicarbonate is more easily detectable due to its higher abundance at physiological pH.[42,43] A confounder for the measurements of PDH flux is an alternative route of CO_2 fixation by pyruvate carboxylase (PC), which if significant, could lead to an

inaccurate estimation of PDH enzymatic activity using hyperpolarized pyruvate.[44] Therefore, imaging of hyperpolarized pyruvate metabolism can simultaneously probe both cytosolic and mitochondrial metabolism. Many pathological processes can result in alterations in cerebral metabolism. For example, necrosis,[45] inflammatory cell activation,[46] and breakdown of the blood–brain barrier[47] may result in elevated lactate in the CNS, either due to increased transport of pyruvate (as in the case of BBB disruption) or lactate formation (secondary to increased enzymatic exchange). Discussion of these effects in multiple sclerosis, stroke, traumatic brain injury, and brain tumors is found below.

Commonly, the term k_{PL} (the apparent exchange rate constant for pyruvate conversion to lactate) or the lactate-to-pyruvate ratio (Lac:Pyr or LP) is used as a measure of glycolytic activity in the cytosol.[41] In contrast, the term k_{PB} (the apparent rate constant of the irreversible conversion of pyruvate to bicarbonate) or the bicarbonate-to-pyruvate ratio (Bic:Pyr or BP) are used as a measure of mitochondrial TCA cycle activity.

Hyperpolarized ^{13}C-MRI of the healthy and diseased brain

There have been a number of pre-clinical studies assessing the metabolism of hyperpolarized ^{13}C substrates in the healthy and pathological brain, including traumatic brain injury, neuro-oncology, multiple sclerosis, and stroke. Detection of metabolic changes with hyperpolarized MRS is dependent on the magnitude of these alterations

present in the pathological state to be assessed, and small or transient changes may remain undetectable.

Metabolism in the healthy brain

The normal brain has a high basal metabolic rate and a reliance upon glucose oxidation.[48] Initial hyperpolarized ^{13}C-MRI studies have investigated the metabolism of hyperpolarized [1-^{13}C]pyruvate and [2-^{13}C]pyruvate in healthy anaesthetized rodent and macaque brains.[49–52] These studies have demonstrated the anaerobic metabolism of ^{13}C-pyruvate to ^{13}C-lactate in the brain parenchyma, catalyzed by cytosolic LDH, as well as the formation of ^{13}C-bicarbonate secondary to mitochondrial PDH and oxidative metabolism. The latter has been supported by the alternative approach of using [2-^{13}C]pyruvate,[53] which has shown the formation of TCA intermediates. Compared to other metabolically active organs, the apparent rate of metabolism of hyperpolarized pyruvate in the brain is comparatively low ($\sim$0.003 s^{-1}) compared to liver and kidney ($\sim$0.02 and 0.025 s^{-1} respectively),[51,54] which may reflect a limitation of pyruvate transport across the blood–brain barrier (BBB). Studies performed with hyperpolarized [1-^{13}C]ethyl-pyruvate, a lipophilic analogue of pyruvate, have revealed enhanced diffusion-facilitated transport across the BBB and subsequent hydrolysis to pyruvate followed by exchange to lactate, demonstrating that BBB transport of pyruvate may be rate limiting in some species.[47,55,56] There is evidence that the detection of [1-^{13}C]pyruvate metabolism in the anaesthetized porcine brain may to some extent be limited by BBB transport[47] (Figure 3). Furthermore, studies have also assessed the difference in pyruvate to lactate exchange before and after transient opening of the BBB with both mannitol and focused ultrasound, demonstrating elevated exchange after permeabilization.[47,57]

Further pre-clinical healthy brain studies have demonstrated metabolism with other tracers such as [1-^{13}C]lactate to measure MCT1 and LDHA activity, [1-^{13}C]glutamine to measure IDH mutation status, and ketoisocaproic acid (KIC) to probe leucine metabolism.[56,58,59] A further tracer of interest in brain studies could be [1,4-[13]C_2]fumarate, which may inform upon cellular necrosis through exchange to malate.[60] Further probes that may be used in future clinical work have been reviewed elsewhere.[61]

Transport of ^{13}C pyruvate across the anaesthetized blood–brain barrier

Some degree of controversy exists surrounding the rate of transport and metabolism of pyruvate under
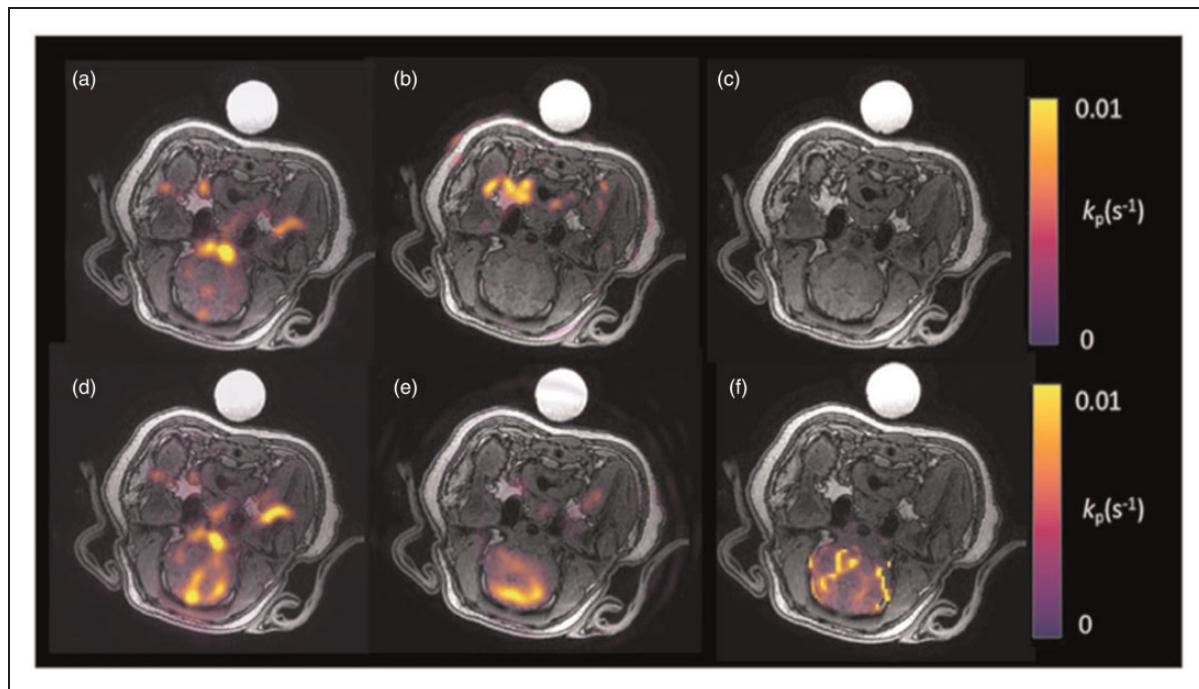
Figure 3. Metabolic imaging of the porcine brain. Imaging of the naïve porcine brain following injection of hyperpolarized ^{13}C-pyruvate. (a) ^{13}C-pyruvate signal is demonstrated in the vasculature. However, no ^{13}C-lactate signal (b) is seen in the brain parenchyma and therefore no significant metabolism is demonstrated on the kinetic rate constant map (c) (k_{PL} in s^{-1}; calculated only in the brain region). After the introduction of mannitol, both ^{13}C-pyruvate (d) and ^{13}C-lactate (e) are seen in the brain parenchyma as demonstrated on the calculated kinetic rate constant map (f). Figure adapted from Miller et al.[47]

differing anaesthetic regimes, with initial work suggesting that the quantities of hyperpolarized ^{13}C-bicarbonate and ^{13}C-lactate detected after the injection of hyperpolarized [1-^{13}C]pyruvate are, to some extent, dependent upon the anaesthetic regimen used.[58] In addition to alterations in transport, anaesthesia may also lead to metabolic shifts: in the heart, increasing the concentration of inhaled isoflurane has been shown to shift cardiac metabolism towards glycolysis, increasing the detected lactate-to-pyruvate ratio and decreasing the signal from bicarbonate.[62] As patients are usually imaged awake, this could influence comparisons between pre-clinical and human results: for example, the low bicarbonate signal detected in the anesthetized brain may be explained by a shift towards glycolysis driven by anaesthesia.[58]

Imaging the healthy human brain with hyperpolarized ^{13}C-MRI and comparison to ^{18}F-FDG PET

Initial clinical studies of healthy brain metabolism have shown the rapid delivery and metabolism of pyruvate to bicarbonate, as well as exchange to lactate in the normal brain parenchyma.[63–65] A recent study of the healthy brain quantified the metabolism of pyruvate in both white and grey matter, with results revealing significantly increased ^{13}C-pyruvate, ^{13}C-lactate, and ^{13}C-bicarbonate in grey matter compared to white matter, which in part may be due to the higher perfusion in the former.[63] However, this regional variation is also likely to relate to real alterations in tissue metabolism as there is increased ^{18}F-FDG uptake on PET in grey matter compared to white matter, which is less dependent on speed of perfusion.[66]

In comparison to hyperpolarized ^{13}C-MRI measurements of pyruvate metabolism, ^{18}F-FDG PET provides a highly sensitive measure of glucose metabolism, particularly the transport and phosphorylation of the FDG glucose analogue by GLUT-1 and hexokinase respectively. However, as PET measures the accumulation of radiolabel, it is unable to discriminate between the injected radiolabelled tracer and downstream metabolic products or their distribution in the cellular or extracellular spaces. Despite the significant increase in SNR afforded by hyperpolarization, it remains significantly less sensitive to the detection of metabolites than PET and in general this means a lower spatial resolution. However, the major strength of HP MRS over PET is the ability to discriminate the injected substrate from its metabolic product or products, allowing a quantitative measure of enzymatic activity. Moreover, although the spatial resolution of HP MRS is insufficient to discriminate between

intracellular and extracellular metabolites, as the formation of hyperpolarized lactate is intracellular, its presence indicates that intracellular metabolism has occurred even if that lactate has been exported to the extracellular space. Another important distinction between the two techniques is the timescale of metabolism that is being assessed as HP MRS detects pyruvate metabolism over seconds to minutes due to the short half-life, whereas PET assesses FDG accumulation over minutes to hours; therefore, the two methods are measuring metabolism on very different timescales. Therefore, the two techniques are highly complementary.

Quantitative modelling has shown that there are regional variations in ^{13}C-pyruvate metabolism across the brain with lower k_{PL} in deep white matter compared to the brainstem and basal ganglia. Interestingly, steady state lactate is not commonly detected in the resting healthy adult brain using ^{1}H-MRS and the difference between this finding and the significant ^{13}C-lactate signal demonstrated with hyperpolarized ^{13}C-MRI may be partly explained by the fact that the latter probes dynamic changes in lactate labelling following the injection of a supraphysiological bolus of pyruvate. Indeed, it may be that the static pool of lactate measured by ^{1}H-MRS is relatively small due to the rapid transport and metabolism of pyruvate in neurons. A further study focusing on the use of [2-^{13}C]pyruvate in the healthy brain has been recently undertaken, with results showing the formation of TCA intermediates dynamically in the parenchyma, particularly glutamate.[67] Example hyperpolarized ^{13}C images from healthy volunteers are seen in Figures 4 and 5.

Further studies with larger cohorts of healthy volunteers at higher spatial resolutions may elucidate other regional differences in the metabolism of the healthy brain, allowing for a better understanding of normal cerebral physiology, as well as providing a baseline for comparison to pathological tissue.

Imaging the diseased brain with hyperpolarized ^{13}C-MRI

There are a number of neurological conditions which could benefit from the application of hyperpolarized ^{13}C-MRI to understand alterations in neurological metabolism due to cerebral insult and therapeutic response. This review will discuss neuro-oncology, multiple sclerosis (MS), traumatic brain injury (TBI) and stroke. Elevation in tissue lactate is a common feature in all of these conditions which raises the potential for the use of hyperpolarized ^{13}C-MRI as a tool to probe metabolism in many neurological conditions.
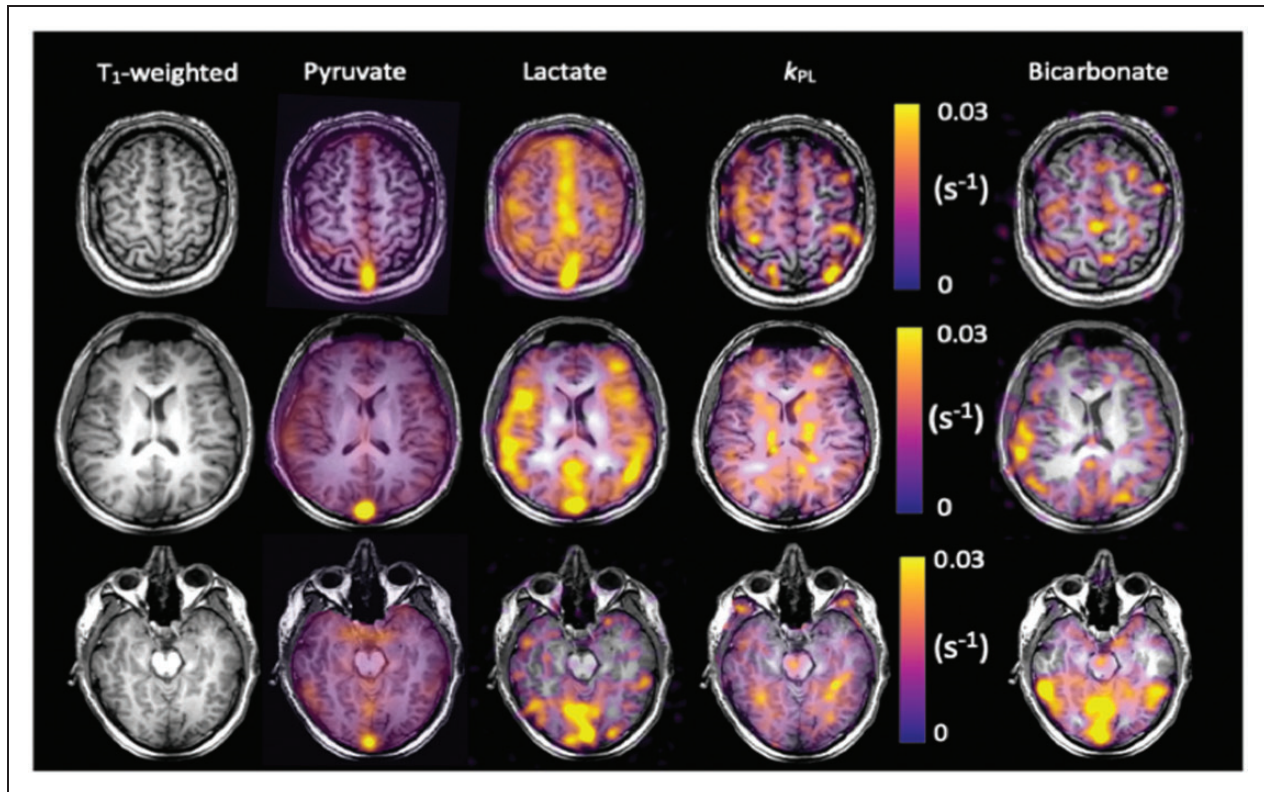
Figure 4. [13]C imaging demonstrating metabolite distribution in the healthy human brain. Example summed images from the brain of a healthy volunteer demonstrating ^{13}C-pyruvate, ^{13}C-lactate, and ^{13}C-bicarbonate signal from three axial slices: superior, central and inferior. The T_1-weighted images have also been shown, as have the quantitative maps of the exchange of pyruvate to lactate (k_{PL} in s^{-1}).[63]
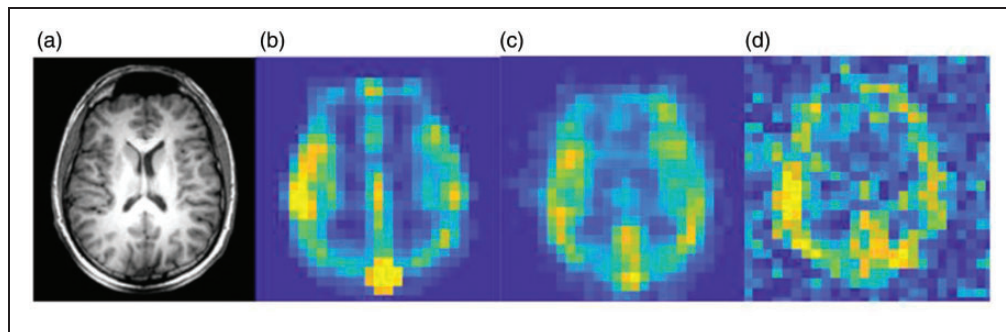

Figure 5. Resolution of ^{13}C imaging of the normal human brain. (a) Proton anatomical imaging. IDEAL spiral Chemical Shift Images (CSI) are shown at the acquired spatial resolution to demonstrate the difference in SNR between: (b) pyruvate; (c) lactate; and (d) bicarbonate. [13]C images are normalized to the metabolite peak signal in the slice. Imaging parameters: field of view = 240 mm, matrix size = 40 × 40, slice thickness = 30 mm. Adapted from Grist et al.[63]

Brain tumors

Several early studies using hyperpolarized [1-^{13}C]pyruvate as a probe for pre-clinical models of brain tumors have demonstrated increased lactate in implanted cerebral tumors, both orthotopic xenograft models in immunocompromised animals and implanted rodent-derived cell cultures in immunocompetent animals.[68–70] Lactate labelling has been shown to correlate with the histological aggressiveness of the tumor and a reduction in lactate labelling has been shown to correspond to therapy response, as chemotherapeutic agents such as temozolomide may have a metabolic effect before a reduction in tumor volume.[56,71] Several studies assessing HP ^{13}C-MRS to detect therapeutic response in neuro-oncology have been undertaken, with reductions in the

lactate signal observed following successful therapies, such as anti-VEGF,[72] telozolomide,[73] dichloroacetate,[74] and radiotherapy.[75] Therefore, the use of hyperpolarized ^{13}C-MRI may be a valuable tool in the monitoring of neuro-oncological disease before and after chemotherapy and radiotherapy. The isocitrate dehydrogenase-1 (IDH-1) mutant status of glioma has been shown to correlate with the metabolism of hyperpolarized [1-^{13}C]alpha-ketoglutarate and its subsequent conversion through the branched-chain amino acid transaminase BCAT1 to [1-^{13}C]glutamate, with the latter being significantly lower in mutant IDH1 cells and tumors.[76] Such reactions form a specific readout of the tumor metabolome and are more challenging to assess with conventional *in vivo* non-invasive methods, such as proton spectroscopy.[77] Therefore, this offers a promising target for non-invasively phenotyping tumors with hyperpolarized ^{13}C-MRI.

Initial human studies have assessed the feasibility of using hyperpolarized [1-^{13}C]pyruvate to probe brain tumor metabolism.[21,78] In keeping with the many preclinical studies in this field, this work has shown that there is significant conversion of pyruvate to lactate in a diverse range of tumors such as high grade glioma,[75] oligodendroglioma[79] and melanoma metastases.[79] However, there is a high degree of variation in lactate labelling between tumors, reflecting the complex heterogeneity of human tumors in comparison to animal models.[21,78] This preliminary evidence provides some initial evidence for the potential role for the technique in studying brain tumors and future work will address the significance of the technique.

Multiple sclerosis

Multiple Sclerosis (MS) is characterized by inflammation of the central nervous system, leading to inflammatory demyelination of neurons and oligodendrocyte death, and subsequently elevated metabolic demands on neurons caused by a toxic elevation of extracellular ions such as calcium and sodium.[80] Preclinically, hyperpolarized ^{13}C-MRS has been used to characterize a cuprizone model of MS, which reproducibly develops inflammatory lesions that attract proinflammatory mononuclear phagocytes, particularly in the corpus callosum, similar to the human disorder.[81] An elevated lactate signal was demonstrated within MS lesions that were histologically confirmed to be rich in mononuclear phagocytes. Moreover, these activated proinflammatory mononuclear phagocytes had elevated pyruvate dehydrogenase kinase 1 (PDK1), responsible for inhibition of the oxidation of pyruvate by mitochondrial PDH, leading to increased metabolism to lactate in the cytosol. As well as furthering our understanding of lesional metabolism, hyperpolarized ^{13}C-MRI could

provide key insights into the viability of normal appearing tissue in the MS brain, through the assessment of lactate exchange and bicarbonate metabolism in normal appearing white and grey matter.

Traumatic brain injury

Acute TBI produces characteristic metabolic changes in the brain, both locally and remote to the site of injury, with elevated lactate detected with ^{1}H-MRS.[82,83] As TBI is known to actively inhibit PDH activity and initiate mitochondrial dysfunction within 4 h after injury,[84] hyperpolarized pyruvate may potentially form a useful metric for understanding and quantifying the degree of injury sustained.[85] TBI is a major cause of death and long-term disability, characterized by cognitive and memory impairment, mood disorders and neurodegenerative diseases.

Non-invasively detecting the spatial distribution of this metabolic dysregulation is challenging with conventional MRS and consequently invasive measures have been used to characterize this heterogeneity.[86] Initial preclinical results with hyperpolarized [1-^{13}C]pyruvate have shown regional alterations in lactate and bicarbonate formation after TBI, reporting a ~24% decrease in oxidative metabolism at the injury site and a concomitant increase in lactate production.[85] Interestingly, there is some evidence that pyruvate or ethyl-pyruvate administration alone may be neuroprotective following TBI in the rat, albeit at higher doses than are typically used for hyperpolarized imaging experiments.[87]

Stroke

Hyperpolarized ^{13}C-MRI may have a significant role in understanding the development and response of the ischemic penumbra in stroke. A pre-clinical endothelin-1-induced ischaemic stroke model has been used to assess the metabolic alterations following acute ischaemic stroke in rats.[49] The results showed an increase in total lactate production in the ischemic penumbra compared to the contralateral brain, which can partly be attributed to increased pyruvate supply and partly to LDH-mediated lactate formation. It is known that ischemia is a gradual process characterized by an intermediate stage in which the metabolic activity of the penumbral tissue is impaired but the damage is reversible and there is therefore the potential for complete functional recovery if blood flow is restored.[4] Currently, the ischemic penumbra is identified by the mismatch between perfusion and diffusion on MRI; however, as the penumbra has a high rate of glucose extraction characterized by anaerobic glycolysis and subsequent elevated lactate production, this could be detected through the altered metabolism of hyperpolarized ^{13}C-pyruvate.[88] Indeed,

invasive studies have shown that a measurement of metabolic activity in the penumbra may be more sensitive than conventional imaging approaches when estimating penumbral viability.[89] Therefore, since hyperpolarized ^{13}C-MRI can identify and quantify the dynamic production of lactate, it may be used to better visualize and characterize the penumbra, in a non-invasive fashion. However, studies focusing on longitudinal measurements of penumbral metabolism are required to understand the true potential of hyperpolarized[13]C-MRI to detect early response of the penumbra to treatment.

Concluding remarks

In conclusion, hyperpolarized ^{13}C-MRI provides a highly sensitive technique to directly and non-invasively probe the dynamics of tissue metabolism *in vivo* and offers the possibility to undertake novel *in vivo* biological explorations of neurological disease. The temporal and spatial resolution of conventional proton MR spectroscopy has been limited by low signal-to-noise, but the very significant increase in signal afforded by hyperpolarized ^{13}C-MRI has allowed the cerebral metabolism of ^{13}C-pyruvate to be probed in real time. The technique has applications in a wide spectrum of diseases where metabolic status is impaired, reprogrammed or jeopardised. This method has revealed new insights into cerebral metabolism and offers a novel approach to study neurological disease, in particular the interplay between aerobic and anaerobic metabolism as seen in diseases as diverse as stroke, multiple sclerosis and brain tumors.

Authors' contributions

JG, JJM, FZ, FAGl wrote the manuscript; JG, JJM, FZ, MAM, FR, TM, DJT, CL, AJC, and FAG were in charge of reviewing the manuscript.

Authors' note

References included in this review article were chosen from PubMed using the terms "brain" "hyperpolarization", and "MRI." There were no language restrictions. The final reference list was generated on the basis of relevance to the topics covered in this review.

ORCID iD

James T Grist [ID] https://orcid.org/0000-0001-7223-4031

References

1. Orphanidou-Vlachou E, Auer D, Brundler MA, et al. [1]H magnetic resonance spectroscopy in the diagnosis of paediatric low grade brain tumours. *Eur J Radiol* 2013; 82: e295–e301.
2. Tomiyasu M, Aida N, Shibasaki J, et al. Normal lactate concentration range in the neonatal brain. *Magn Reson Imaging* 2016; 34: 1269–1273.
3. Zhu X, Cao L, Hu X, et al. Brain metabolism assessed via proton magnetic resonance spectroscopy in patients with amnestic or vascular mild cognitive impairment. *Clin Neurol Neurosurg* 2014; 130: 80–85.
4. Bivard A, Krishnamurthy V, Stanwell P, et al. Spectroscopy of reperfused tissue after stroke reveals heightened metabolism in patients with good clinical outcomes. *J Cereb Blood Flow Metab* 2014; 34: 1944–1950.
5. Coles JP, Cunningham AS, Salvador R, et al. Early metabolic characteristics of lesion and nonlesion tissue after head injury. *J Cereb Blood Flow Metab* 2009; 29: 965–975.
6. Faghihi R, Zeinali-Rafsanjani B, Mosleh-Shirazi MA, et al. Magnetic resonance spectroscopy and its clinical applications: a review. *J Med Imaging Radiat Sci* 2017; 48: 233–253.
7. Verma A, Kumar I, Verma N, et al. Magnetic resonance spectroscopy - Revisiting the biochemical and molecular milieu of brain tumors. *BBA Clin* 2016; 5: 170–178.
8. Wilson M, Andronesi O, Barker PB, et al. A methodological consensus on clinical proton MR spectroscopy of the brain: review and recommendations. 2019; 82: 527–550.
9. Sailasuta N, Robertson LW, Harris KC, et al. Clinical NOE 13C MRS for neuropsychiatric disorders of the frontal lobe. *J Magn Reson* 2008; 195: 219–25.
10. Gruetter R, Novotny J, Boulware SD, et al. Localized ^{13}C NMR spectroscopy in the human brain of amino acid labeling from D- [1- ^{13}C] glucose. *J Neurochem* 63: 1377–1385.
11. Wijnen JP, Van der Graaf M, Scheenen TWJ, et al. In vivo 13C magnetic resonance spectroscopy of a human brain tumor after application of ^{13}C-1-enriched glucose. *Magn Reson Imaging* 2010; 28: 690–697.
12. Sonnay S, Poirot J, Just N, et al. Astrocytic and neuronal oxidative metabolism are coupled to the rate of

glutamate–glutamine cycle in the tree shrew visual cortex. *Glia* 2018; 66: 477–491.

13. Girault FM, Sonnay S, Gruetter R, et al. Alterations of brain energy metabolism in type 2 diabetic Goto-Kakizaki rats measured in vivo by ^{13}C magnetic resonance spectroscopy. *Neurotox Res* 2019; 36: 268–278.

14. Cheshkov S, Dimitrov IE, Jakkamsetti V, et al. Oxidation of [U-^{13}C]glucose in the human brain at 7T under steady state conditions. *Magn Reson Med* 2017; 78: 2065–2071.

15. De Feyter HM, Herzog RI, Steensma BR, et al. Selective proton-observed, carbon-edited (selPOCE) MRS method for measurement of glutamate and glutamine ^{13}C-labeling in the human frontal cortex. *Magn Reson Med* 2018; 80: 11–20.

16. Ardenkjaer-Larsen JH, Fridlund B, Gram A, et al. Increase in signal-to-noise ratio of >10,000 times in liquid-state NMR. *Proc Natl Acad Sci U S A* 2003; 100: 10158–63.

17. Gallagher FA, Bohndiek SE, Kettunen MI, et al. Hyperpolarized 13C MRI and PET: in vivo tumor biochemistry. *J Nucl Med* 2011; 52: 1333–1336.

18. Golman K, Olsson LE, Axelsson O, et al. Molecular imaging using hyperpolarized ^{13}C. *Br J Radiol* 2003; 76: S118–S127.

19. Keshari KR and Wilson DM. Chemistry and biochemistry of 13C hyperpolarized magnetic resonance using dynamic nuclear polarization. *Chem Soc Rev* 2014; 43: 1627–1659.

20. Månsson S, Johansson E, Magnusson P, et al. ^{13}C imaging-a new diagnostic platform. *Eur Radiol* 2006; 16: 57–67.

21. Park I, Larson PEZ, Gordon JW, et al. Development of methods and feasibility of using hyperpolarized carbon-13 imaging data for evaluating brain metabolism in patient studies. *Magn Reson Med* 2018; 80: 864–873.

22. Nelson SJ, Kurhanewicz J, Vigneron DB, et al. Metabolic imaging of patients with prostate cancer using hyperpolarized [1-^{13}C]Pyruvate. *Sci Transl Med* 2013; 487: 109–113.

23. Aggarwal R, Vigneron DB and Kurhanewicz J. Hyperpolarized 1-[^{13}C]-pyruvate magnetic resonance imaging detects an early metabolic response to androgen ablation therapy in prostate cancer. *Eur Urol* 2017; 72: 1028–1029.

24. Cunningham CH, Lau JYC, Chen AP, et al. Hyperpolarized ^{13}C metabolic MRI of the human heart: initial experience. *Circ Res* 2016; 119: 1177–1182.

25. von Morze C, Bok RA, Sands JM, et al. Monitoring urea transport in rat kidney in vivo using hyperpolarized ^{13}C magnetic resonance imaging. *Am J Physiol Ren Physiol* 2012; 302: 1658–1662.

26. Qi H, Mariager CØ, Nielsen PM, et al. Glucagon infusion alters the hyperpolarized ^{13}C-urea renal hemodynamic signature. *NMR Biomed* 2018; 32: e4028.

27. Qi H, Nørlinger TS, Nielsen PM, et al. Early diabetic kidney maintains the corticomedullary urea and sodium gradient. *Physiol Rep* 2016; 4: 1–6.

28. Reed GD, Morze C Von, Verkman AS, et al. Imaging renal urea handling in rats at millimeter resolution using hyperpolarized magnetic resonance relaxometry. *Tomography* 2016; 2: 125–137.

29. Mariager CØ, Nielsen PM, Qi H, et al. Hyperpolarized ^{13}C, $^{15}N_2$-urea T_2 relaxation changes in acute kidney injury. *Magn Reson Med* 2017; 702: 696–702.

30. Nielsen PM, Eldirdiri A, Bertelsen LB, et al. Fumarase activity: an in vivo and in vitro biomarker for acute kidney injury. *Sci Rep* 2017; 7: 40812.

31. Grist JT, Mariager CØ, Qi H, et al. Detection of acute kidney injury with hyperpolarized [^{13}C, ^{15}N]Urea and multiexponential relaxation modeling. *Magn Reson Med*, Epub ahead of print 15 December 2019. DOI: 10.1002/mrm.28134.

32. Zaccagna F, Grist JT, Deen SS, et al. Hyperpolarized carbon-13 magnetic resonance spectroscopic imaging: a clinical tool for studying tumour metabolism. *Br J Radiol* 2018; 91: 1–11.

33. Wang J, Wright AJ, Hesketh RL, et al. A referenceless Nyquist ghost correction workflow for echo planar imaging of hyperpolarized [1-^{13}C]pyruvate and [1-^{13}C]lactate. *NMR Biomed* 2017; 32: e3866.

34. Le Page LM, Ball DR, Ball V, et al. Simultaneous in vivo assessment of cardiac and hepatic metabolism in the diabetic rat using hyperpolarized MRS. *NMR Biomed* 2016; 29: 1759–1767.

35. Gordon JW, Hansen RB, Shin PJ, et al. 3D hyperpolarized C-13 EPI with calibrationless parallel imaging. *J Magn Reson* 2018; 289: 92–99.

36. Lau AZ, Chen AP, Ghugre NR, et al. Rapid multislice imaging of hyperpolarized ^{13}C pyruvate and bicarbonate in the heart. *Magn Reson Med* 2010; 64: 1323–1331.

37. Vinding MS, Laustsen C, Maximov II, et al. Dynamic nuclear polarization and optimal control spatial-selective13C MRI and MRS. *J Magn Reson* 2013; 227: 57–61.

38. Larson PEZ, Kerr AB, Chen AP, et al. Multiband excitation pulses for hyperpolarized 13C dynamic chemical-shift imaging. *J Magn Reson* 2008; 194: 121–127.

39. Schmidt R, Laustsen C, Dumez J-N, et al. In vivo single-shot 13C spectroscopic imaging of hyperpolarized metabolites by spatiotemporal encoding. *J Magn Reson* 2014; 240: 8–15.

40. Durst M, Koellisch U, Frank A, et al. Comparison of acquisition schemes for hyperpolarised ^{13}C imaging. *NMR Biomed* 2015; 28: 715–725.

41. Daniels CJ, Mclean MA, Schulte RF, et al. A comparison of quantitative methods for clinical imaging with hyperpolarized ^{13}C-pyruvate. *NMR Biomed* 2016; 29: 387–399.

42. Gallagher FA, Kettunen MI, Day SE, et al. Magnetic resonance imaging of pH in vivo using hyperpolarized ^{13}C-labelled bicarbonate. *Nature* 2008; 453: 940–943.

43. Gallagher FA, Sladen H, Kettunen MI, et al. Carbonic anhydrase activity monitored in vivo by hyperpolarized ^{13}C-magnetic resonance spectroscopy demonstrates its importance for ph regulation in tumors. *Cancer Res* 2015; 75: 4109–4118.

44. Siddiqui S, Kadlecek S, Pourfathi M, et al. The use of hyperpolarized carbon-13 magnetic resonance for molecular imaging. *Adv Drug Deliv Rev* 2017; 113: 3–23.

45. Bohndiek SE, Kettunen MI, Hu D, et al. Detection of tumor response to a vascular disrupting agent by

hyperpolarized ^{13}C magnetic resonance spectroscopy. *Mol Cancer Ther* 2010; 9: 3278–3288.

46. Grist JT, Jarvis LB, Georgieva Z, et al. Extracellular lactate: a novel measure of t cell proliferation. *J Immunol* 2018; 200: 1220–1226.

47. Miller JJ, Grist JT, Serres S, et al. ^{13}C pyruvate transport across the blood-brain barrier in preclinical hyperpolarised MRI. *Sci Rep* 2018; 8: 15082.

48. Kaphingst KA, Persky S and Lachance C. Brain: normal variations and benign findings in FDG PET/CT imaging. *PET Clin* 2010; 14: 384–399.

49. Xu Y, Ringgaard S, Østergaard Mariager C, et al. Hyperpolarized ^{13}C magnetic resonance imaging can detect metabolic changes characteristic of penumbra in ischemic stroke. *Tomography* 2017; 3: 67–73.

50. Chen Y, Kim H, Bok R, et al. Pyruvate to lactate metabolic changes during neurodevelopment measured dynamically using hyperpolarized ^{13}C imaging in juvenile murine brain. *Dev Neurosci* 2016; 38: 34–40.

51. Park I, Larson PEZ, Tropp JL, et al. Dynamic hyperpolarized carbon-13 MR metabolic imaging of nonhuman primate brain. *Magn Reson Med* 2014; 71: 19–25.

52. Mayer D, Yen Y-F, Takahashi A, et al. Dynamic and high-resolution metabolic imaging of hyperpolarized [1-^{13}C]-pyruvate in the rat brain using a high-performance gradient insert. *Magn Reson Med* 2011; 65: 1228–1233.

53. Park JM, Josan S, Grafendorfer T, et al. Measuring mitochondrial metabolism in rat brain in vivo using MR Spectroscopy of hyperpolarized [2-^{13}C]pyruvate. *NMR Biomed* 2013; 26: 1197–1203.

54. Bahrami N, Swisher CL, Von Morze C, et al. Kinetic and perfusion modeling of hyperpolarized ^{13}C pyruvate and urea in cancer with arbitrary RF flip angles. *Quant Imaging Med Surg* 2014; 4: 24–32.

55. Hurd RE, Yen Y, Mayer D, et al. Metabolic imaging in the anesthetized rat brain using hyperpolarized [1-^{13}C] pyruvate and [1-^{13}C] ethyl pyruvate. *Magn Reson Med* 2011; 63: 1137–1143.

56. Takado Y, Cheng T, Bastiaansen JAM, et al. Hyperpolarized 13C MRS reveals the rate-limiting role of the blood-brain barrier on the cerebral uptake and metabolism of L-lactate in vivo. *ACS Chem Neurosci* 2018; 9: 2554–2562.

57. Mishkovsky M, Lengacher S and Comment A. Hyperpolarized ^{13}C magnetic resonance spectroscopy reveals the rate-limiting role of the blood–brain barrier in the cerebral uptake and metabolism of L-lactate in vivo. *ACS Chem Neurosci* 2018; 9: 2554–2562.

58. Josan S, Hurd R, Billingsley K, et al. Effects of isoflurane anesthesia on hyperpolarized 13C metabolic measurements in rat brain. *Magn Reson Med* 2013; 70: 1117–1124.

59. Chaumeil MM, Larson PEZ, Woods SM, et al. Hyperpolarized [1-^{13}C] glutamate: a metabolic imaging biomarker of IDH1 mutational status in glioma. *Cancer Res* 2014; 74: 4247–4257.

60. Gallagher FA, Kettunen MI, Hu D-E, et al. Production of hyperpolarized [1,4-^{13}C$_2$]malate from [1,4-^{13}C$_2$]fumarate is a marker of cell necrosis and treatment response in tumors. *Proc Natl Acad Sci U S A* 2009; 106: 19801–19806.

61. Chaumeil MM, Najac C and Ronen SM. Studies of metabolism using ^{13}C MRS of hyperpolarized probes. *Methods Enzymol* 2015; 561: 1–71.

62. Steinhauser J, Wespi P, Kwiatkowski G, et al. Assessing the influence of isoflurane anesthesia on cardiac metabolism using hyperpolarized [1-^{13}C]pyruvate. *NMR Biomed* 2018; 31: e3856.

63. Grist JT, McLean MA, Riemer F, et al. Quantifying normal human brain metabolism using hyperpolarized [1-^{13}C]pyruvate and magnetic resonance imaging. *Neuroimage* 2019; 189: 171–179.

64. Tang S, Milshteyn E, Reed G, et al. A regional bolus tracking and real-time B1 calibration method for hyperpolarized ^{13}C MRI. *Magn Reson Med* 2019; 81: 839–851.

65. Lee CY, Soliman H, Geraghty BJ, et al. Lactate topography of the human brain using hyperpolarized ^{13}C-MRI. *Neuroimage* 2019; 204: 116202.

66. Arakawa S, Wright PM, Koga M, et al. Ischemic thresholds for gray and white matter: A diffusion and perfusion magnetic resonance study. *Stroke* 2006; 37: 1211–1216.

67. Chung BT, Chen HY, Gordon J, et al. First hyperpolarized [2-^{13}C]pyruvate MR studies of human brain metabolism. *J Magn Reson* 2019; 309: 106617.

68. Park I, Larson PEZ, Zierhut ML, et al. Hyperpolarized 13C magnetic resonance metabolic imaging: application to brain tumors. *Neuro Oncol* 2010; 12: 133–144.

69. Park I, Hu S, Bok R, et al. Evaluation of heterogeneous metabolic profile in an orthotopic human glioblastoma xenograft model using compressed sensing hyperpolarized 3D ^{13}C magnetic resonance spectroscopic imaging. *Magn Reson Med* 2013; 70: 33–39.

70. Harrison C, Yang C, Jindal A, et al. Comparison of kinetic models for analysis of pyruvate-to-lactate exchange by hyperpolarized ^{13}C NMR. *NMR Biomed* 2012; 25: 1286–1294.

71. Park I, Bok R, Ozawa T, et al. Detection of early response to temozolomide treatment in brain tumors using hyperpolarized ^{13}C MR metabolic imaging. *J Magn Reson Imaging* 2011; 33: 1284–1290.

72. Rutering J, Ilmer M, Recio A, et al. Hyperpolarized ^{13}C lactate-to-bicarbonate ratio as a biomarker for monitoring acute response of anti-VEGF treatment. *Nat Rev Drug Discov* 2016; 5: 1–8.

73. Ahn H, Weaver M, Lyon D, et al. Detection of early response to temozolomide treatment in brain tumors using hyperpolarized ^{13}C MR metabolic imaging. *J Magn Reson Imaging* 2011; 33: 1284–1290.

74. Park JM, Recht LD, Josan S, et al. Metabolic response of glioma to dichloroacetate measured in vivo by spectroscopic imaging. *Neuro Oncol* 2013; 15: 433–441.

75. Day SE, Kettunen MI, Cherukuri MK, et al. Detecting response of rat C6 glioma tumors to radiotherapy using hyperpolarized [1-^{13}C]pyruvate and ^{13}C magnetic resonance spectroscopic imaging. *Magn Reson Med* 2011; 65: 557–563.

76. Izquierdo-Garcia JL, Cai LM, Chaumeil MM, et al. Glioma cells with the IDH1 mutation modulate

metabolic fractional flux through pyruvate carboxylase. *PLoS One* 2014; 9: 1–10.

77. Natsumeda M, Igarashi H, Motohashi K, et al. Advances and challenges in assessing 2-hydroxyglutarate in gliomas by magnetic resonance spectroscopy: a short review. *Neuropsychiatry* 2018; 8: 1831–1838.

78. Miloushev VZ, Granlund KL, Boltyanskiy R, et al. Metabolic imaging of the human brain with hyperpolarized ^{13}C pyruvate demonstrates ^{13}C lactate production in brain tumor patients. *Cancer Res* 2018; 78: 3755–3760.

79. Miloushev VZ, Granlund KL, Boltyanskiy R, et al. Metabolic imaging of the human brain with hyperpolarized ^{13}C Pyruvate demonstrates ^{13}C lactate production in brain tumor patients. *Cancer Res* 2018; 78: 3755–3760.

80. Mahad D, Lassmann H and Turnbull D. Review: mitochondria and disease progression in multiple sclerosis. *Neuropathol Appl Neurobiol* 2008; 34: 577–589.

81. Guglielmetti C, Najac C, Van Der Linden A, et al. Hyperpolarized ^{13}C MR metabolic imaging can detect neuroinflammation in vivo in a preclinical model of multiple sclerosis. *PNAS* 2017; 18: E6982–E6991.

82. Dhillon HS, Dose JM, Scheff SW, et al. Time course of changes in lactate and free fatty acids after experimental brain injury and relationship to morphologic damage. *Exp Neurol* 1997; 146: 240–249.

83. Guglielmetti C, Chou A, Krukowski K, et al. In vivo metabolic imaging of traumatic brain injury. *Sci Rep* 2017; 7: 17525.

84. Robertson CL, Saraswati M and Fiskum G. Mitochondrial dysfunction early after traumatic brain injury in immature rats. *J Neurochem* 2007; 101: 1248–1257.

85. DeVience SJ, Lu X, Proctor J, et al. Metabolic imaging of energy metabolism in traumatic brain injury using hyperpolarized [1-^{13}C]pyruvate. *Sci Rep* 2017; 7: 1907.

86. Carpenter KLH, Jalloh I, Gallagher CN, et al. ^{13}C-labelled microdialysis studies of cerebral metabolism in TBI patients. *Eur J Pharm Sci* 2014; 57: 87–97.

87. Moro N and Sutton RL. Beneficial effects of sodium or ethyl pyruvate after traumatic brain injury in the rat. *Exp Neurol* 2010; 225: 391–401.

88. Dani KA and Warach S. Metabolic imaging of ischemic stroke: the present and future. *AJNR Am J Neuroradiol* 2014; 35: S37–S43.

89. Pinczolits A, Zdunczyk A, Dengler NF, et al. Standard-sampling microdialysis and spreading depolarizations in patients with malignant hemispheric stroke. *J Cereb Blood Flow Metab* 2017; 37: 1896–1905.